## Supplementary Information:

**Supplementary table 1. NMR and refinement statistics for the solution structures of the RNA duplex with and without SMN-C5.**

| | RNA duplex | RNA duplex-SMN-C5 |
|---|---|---|
| **NMR distance and dihedral constraints** | | |
| Distance restraints | | |
| Total NOE | 355 | 359 |
| Intra-residue | 263 | 278 |
| Inter-residue | 92 | 91 |
| Sequential ($\|i-j\|=1$) | 86 | 85 |
| Nonsequential ($\|i-j\|>1$ ) | 6 | 6 |
| Hydrogen bonds | 18 | 18 |
| Ligand–nucleic acid intermolecular | | 16 |
| Total dihedral angle restraints | 164 | 146 |
| Base pair | 42 | 44 |
| Sugar pucker | 44 | 43 |
| Backbone | 78 | 59 |
| Based on A-form geometry | | |
| **Structure statistics** | | |
| Violations (mean and s.d.) | | |
| Distance constraints (> 0.3Å) | 0.05 ± 0.21 | 0.20 ± 0.40 |
| Dihedral angle constraints (> 5º) | 0 | 0 |
| Max. dihedral angle violation (º) | 0.64 ± 0.04 | 0.61 ± 0.26 |
| Max. distance constraint violation (Å) | 0.28 ± 0.01 | 0.28 ± 0.03 |
| Deviations from idealized geometry | | |
| Bond lengths (Å) | 0.0045 ± 0.0001 | 0.0054 ± 0.0002 |
| Bond angles (º) | 2.06 ± 0.01 | 2.33 ± 0.01 |
| Impropers (º) | | |
| Average pairwise r.m.s. deviation** (Å) | | |
| All RNA heavy | 0.91 ± 0.53 | 1.27 ± 0.64 |
| SMN-C5 binding site | | 0.86 ± 0.28 |
| All nucleotides | 1.32 ± 0.58 | 1.80 ± 0.73 |

**Pairwise r.m.s. deviation was calculated among 20 refined structures.
***SMN-C5 binding site includes nucleotides 7-9 and nucleotides -2 to +2 from the U1 snRNA and the E7 5'-SS.

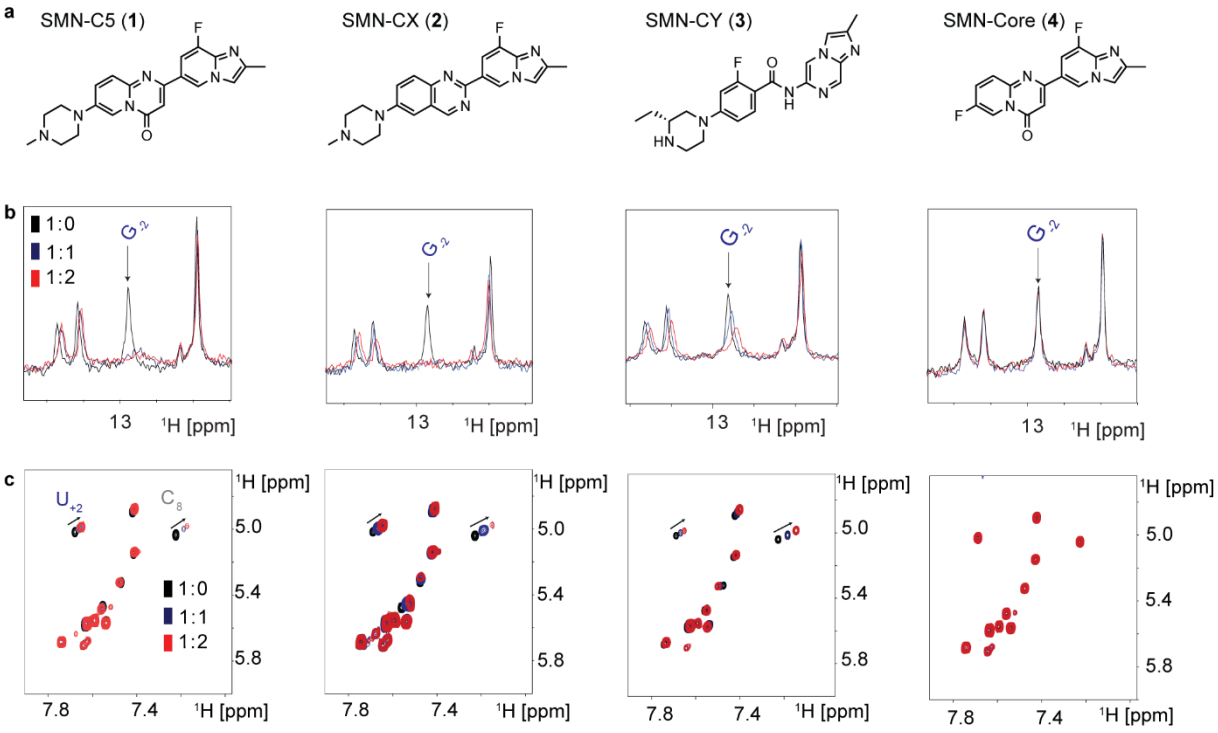


**Supplementary Figure 1 – Interactions between SMN2 splicing modifiers and the RNA duplex. a,** Planar structures of the four splicing modifiers used in this study (SMN-C5, SMN-CX, SMN-CY and SMN-Core). **b,** Changes in the imino region of the 1D $^{1}$H NMR spectra of the RNA observed upon addition of the splicing modifiers. The NMR spectra are colored according to the ratio RNA:compound indicated in the first panel. This experiments have been replicated at least three times with similar results. The position of the signal corresponding to the imino proton of $G_{-2}$ is labeled. **c,** Changes in the pyrimidine region (H5-H6) of the 2D $^{1}$H-$^{1}$H TOCSY NMR spectra of the RNA observed upon addition of the splicing modifiers. The NMR spectra are colored according to the ratio RNA:compound indicated in the first panel. This experiments have been replicated three times with similar results. The positions of the signals of $U_{+2}$ and $C_{8}$ are indicated. The three potent molecules (1, 2 and 3) induced similar chemical shift changes on the NMR spectra of the RNA, suggesting that they interact directly with the RNA in the same binding pocket. In contrast, the inactive compound 4 does not interact with the RNA.

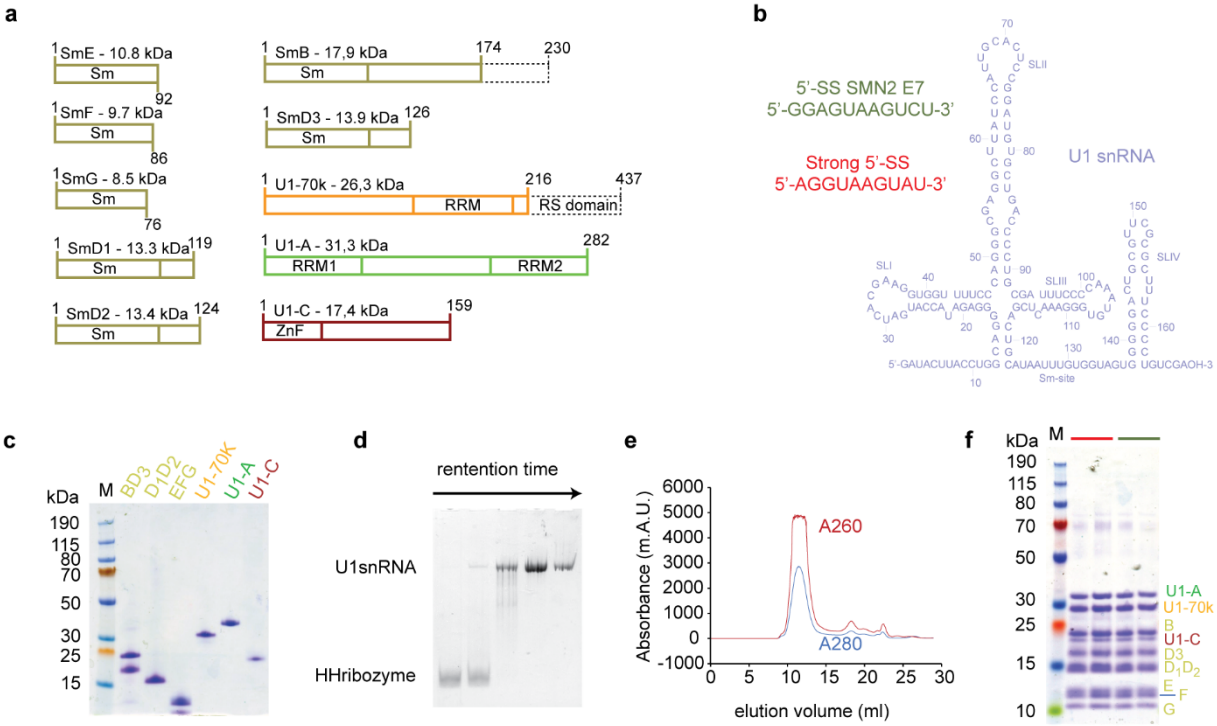


**Supplementary Figure 2 – In vitro reconstitution of U1 snRNP for solution state NMR studies. a,** Schematic representation of the U1 snRNP protein components. Dashes regions were not included in our constructs. **b,** Primary sequences of the RNAs used in this study. **c,** SDS-PAGE gel showing the purified protein components of U1 snRNP. **d,** 12%-Urea-PAGE stained with toluidine showing the separation of the hammerhead ribozyme from the U1 snRNA using ion exchange chromatography in denaturing conditions. **e,** Chromatogram of the size exclusion purification performed to purify U1 snRNP. **f,** SDS-PAGE gel showing the protein compositions of the purified U1 snRNP complexes. The reconstitution of U1 snRNP has been performed two times with similar results.

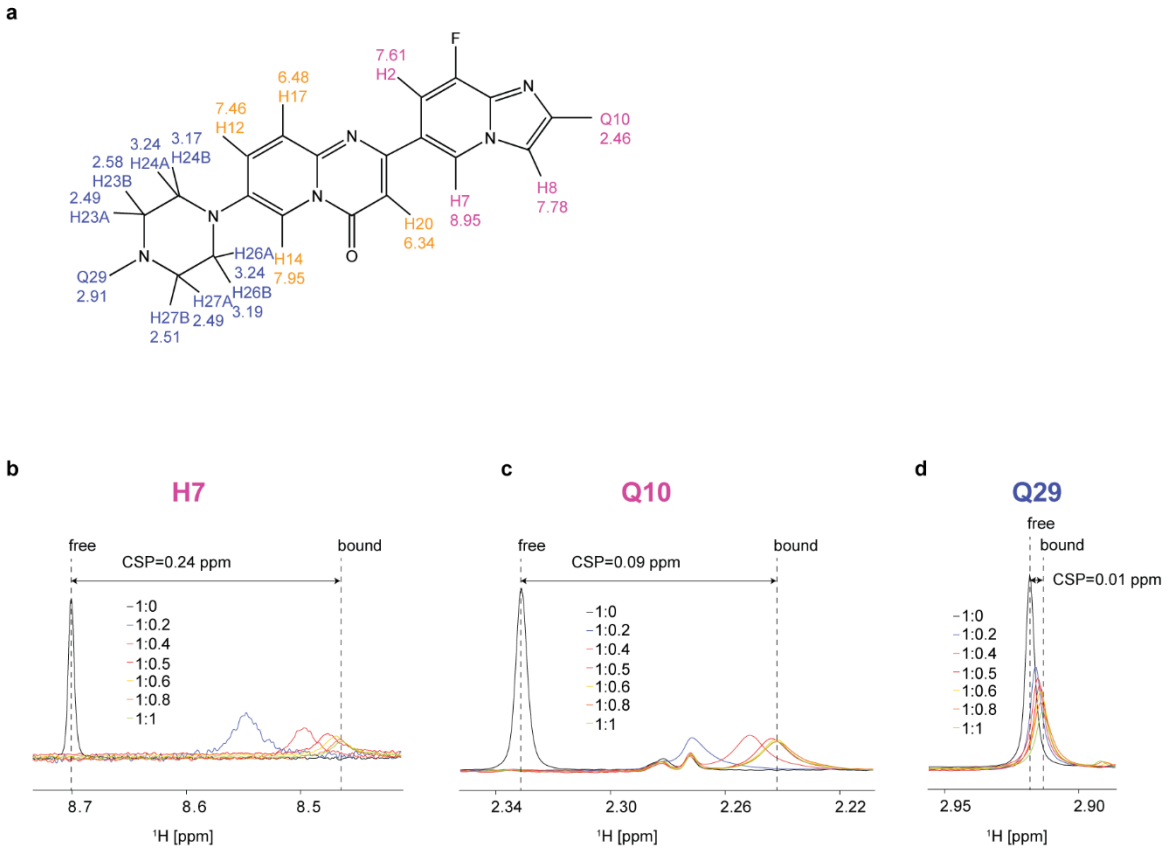


**Supplementary Figure 3 – Binding of SMN-C5 to the RNA duplex. a,** Planar structure of SMN-C5 on which the predicted chemical shifts and atom names are depicted. **b-d,** Overlays of the 1D $^{1}$H spectra of SMN-C5 as a function of the RNA concentration. Each panel shows the change in chemical shifts of one proton from the molecule as a function of the RNA concentration. The NMR spectra are colored according to the SMN-C5:RNA molar ratios. This experiment has been performed two times with similar results.

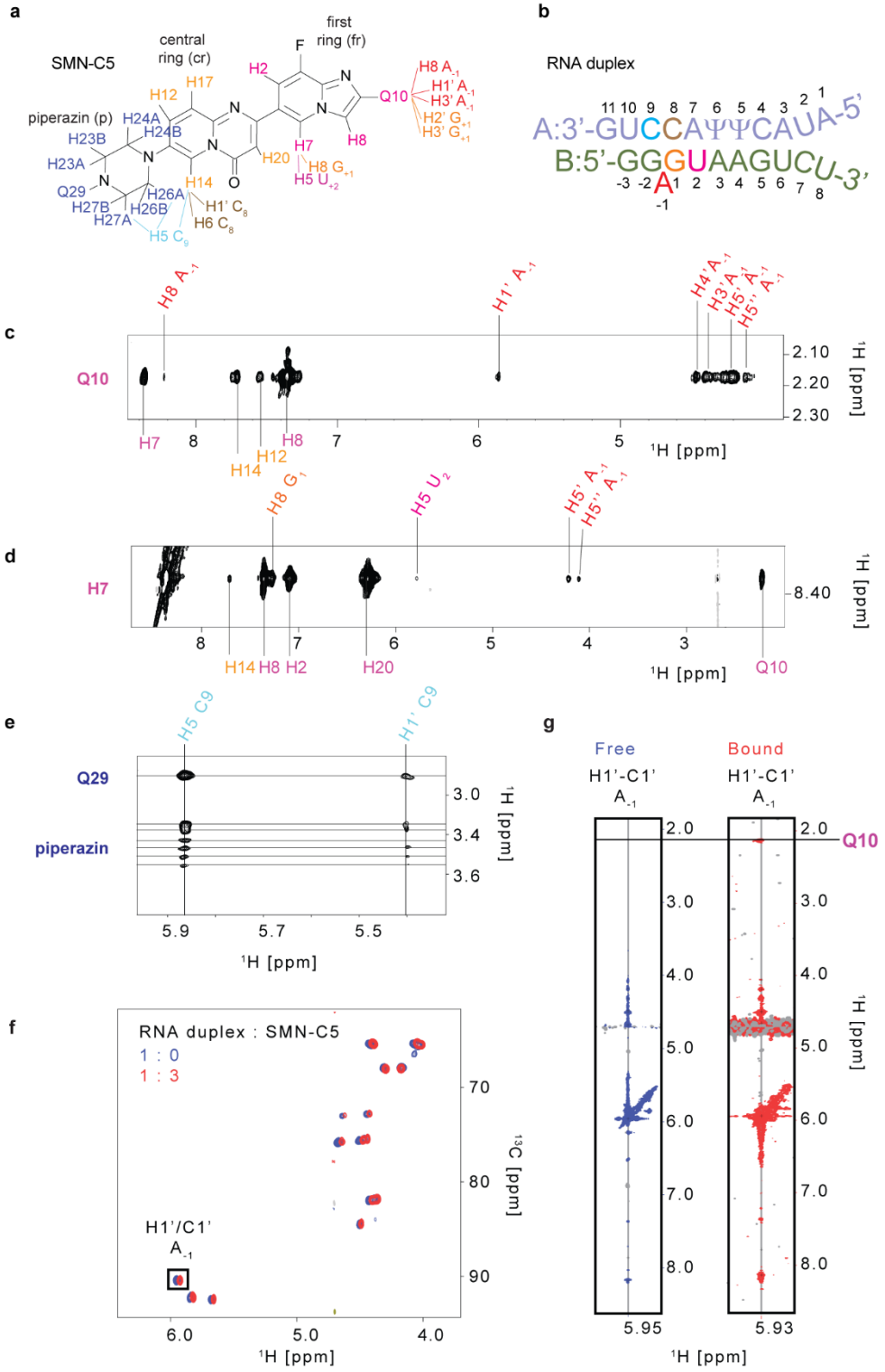


**Supplementary Figure 4 – Identification of intermolecular NOE-derived distances. a,** Planar structure of SMN-C5 on which the intermolecular NOEs are depicted. **b,** Sequence of the RNA duplex. **c,** Region of the 2D $^{1}$H-$^{1}$H NOESY showing the intermolecular NOEs between the methyl group Q10 and the RNA. **d,** Region of the 2D $^{1}$H-$^{1}$H NOESY showing the intermolecular NOEs between the atom H7 and the RNA. **e,** Region of the 2D $^{1}$H-$^{1}$H NOESY showing the intermolecular NOEs between the piperazine group and the RNA. **f,** Overlay of the 2D $^{1}$H-$^{13}$C HSQC spectra of the RNA duplex $^{13}$C-labeled

on the ribose of adenine from the 5'-splice site of *SMN2* E7 recorded with or without SMN-C5. **g,** Part of the 3D $^{1}$H-$^{13}$C HSQC NOESY showing the NOE tower observed for the H1'-C1' couple of $A_{-1}$. The left panel corresponds to the RNA alone while the right panel was recorded in the presence of SMN-C5. On the right NOE tower, an intermolecular NOE between H1' of $A_{-1}$ and the SMN-C5 Q10 pseudo-atom is observed. These NMR experiments have been recorded only once due to the long measurement time required.

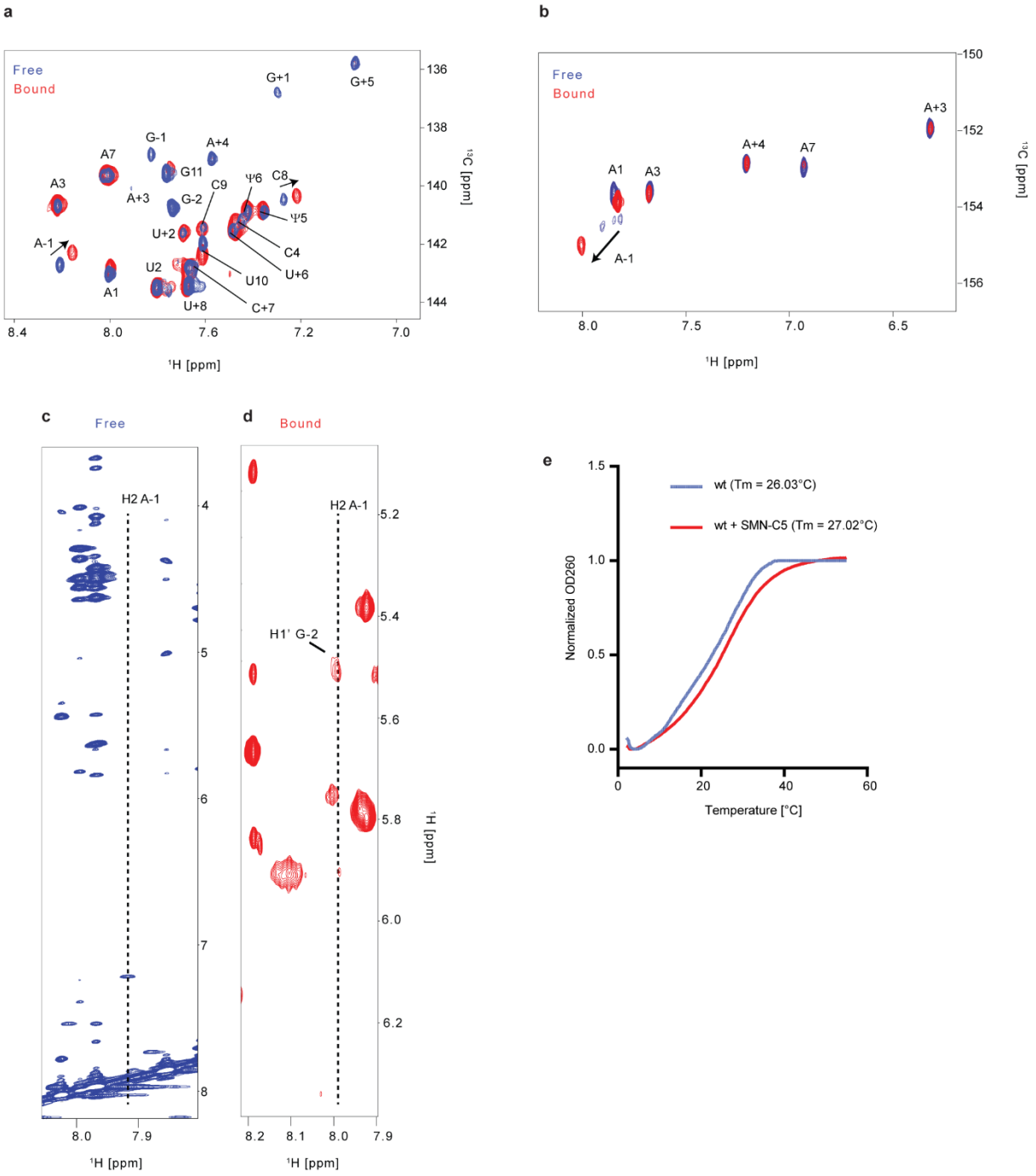


**Supplementary Figure 5 – NMR experimental data showing the stabilization of $A_{-1}$ in the RNA helix base stack. a,** Overlay of the 2D $^{1}H$-$^{13}C$ natural abundance HSQC spectra of the RNA with (red) and without SMN-C5 (blue). The depicted region corresponds to the $H_8$-$C_8$ and $H_6$-$C_6$ groups. This experiment has been recorded one time. **b,** Overlay of the 2D $^{1}H$-$^{13}C$ natural abundance HSQC spectra of the RNA with (red) and without SMN-C5 (blue). The selected region corresponds to the $H_2$-$C_2$ groups of adenines. Upon addition of SMN-C5, the aromatic resonances of $A_{-1}$ are strongly perturbed. This experiment has been recorded one time. **c-d,** Comparison of the intramolecular NOEs observed for the $H_2$ proton of $A_{-1}$ on the 2D $^{1}H$-$^{1}H$ NOESY experiments recorded with (red) and without SMN-C5 (blue). In the presence of SMN-C5, the $H_2$ of $A_{-1}$ shows NOE with the $H_{1'}$ of $G_{-2}$ in line with its shift into the RNA base stack helix. This experiment has been recorded one time since it requires long measurement time. **e,** UV melting curve of the RNA duplex recorded with (red) and without SMN-C5 (blue). The

drug increases the RNA melting temperature by almost a degree. This experiment has been recorded two times with similar results.

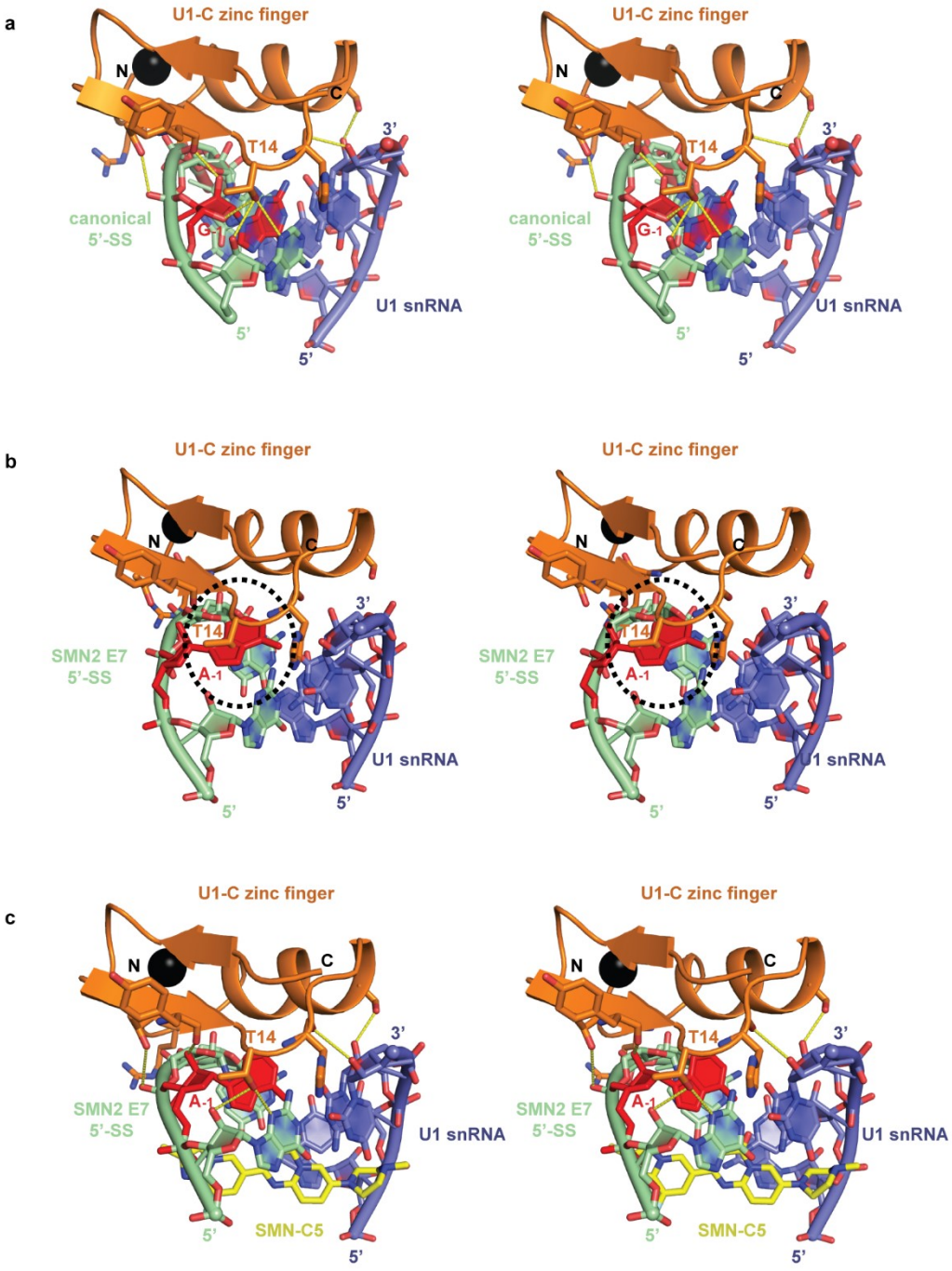


**Supplementary Figure 6 – Modelling of U1-C zinc finger RNA recognition. a,** Stereo view of the RNA helix minor groove recognition by U1-C zinc finger in the high-resolution crystal structure of U1 snRNP[27]. **b,** Stereo view of the model of U1-C zinc finger bound to the RNA duplex formed upon E7 5'-SS recognition. The position of $A_{-1}$ induces an important steric clash with the protein that is shown by the dashed circle. **c,** Stereo view of the model of U1-C zinc finger bound to the RNA duplex in the presence of the splicing modifier. SMN-C5 corrects the position of $A_{-1}$ to prevent the steric clash with the protein. Hydrogen bonds are shown by yellow dashed lines.

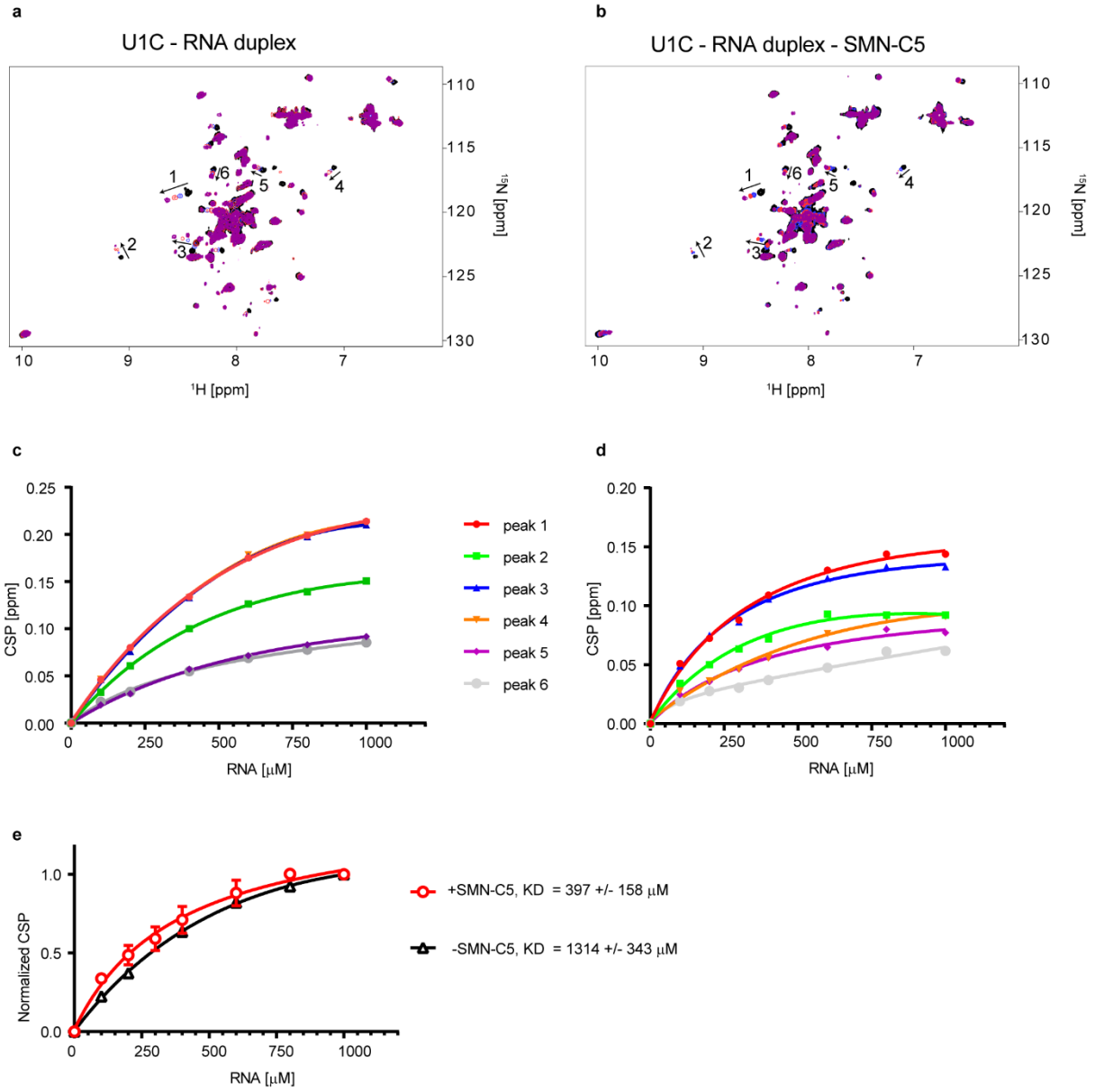


**Supplementary Figure 7 – SMN-C5 promotes the U1-C zinc finger RNA duplex binding activity. a,** Overlay of the 2D $^1$H-$^{15}$N HSQC spectra of the U1-C zinc finger protein (1-61) recorded at different RNA duplex concentrations. The black, blue, red and pink spectra were recorded with 0, 200 µM, 400 µM and 1 mM RNA respectively. The protein concentration was 200 µM. This experiment has been performed in duplicate. **b,** Overlay of the 2D $^1$H-$^{15}$N HSQC spectra of the U1-C zinc finger protein (1-61) recorded at different RNA duplex concentrations in the presence of SMN-C5. The conditions are the same than in **a**. Six NMR signals showing chemical shift changes are labelled on both panels. This experiment has been performed in duplicate. **c,** Plot showing the normalized chemical shift changes of the 6 NMR signals of U1-C in function of the RNA duplex concentration. **d,** Plot showing the normalized chemical shift changes of the 6 NMR signals of U1-C in function of the RNA duplex – SMN-C5 concentration. **e,** Plot showing the normalized and average chemical shift changes of the 6 NMR signals of U1-C as a function of the RNA concentration (n = 6). The open circles correspond to the average and errors bars correspond to

standard deviations. Black and red curves correspond to the data obtained in the absence and in the presence of SMN-C5, respectively. These data demonstrate that SMN-C5 promotes the U1-C zinc finger RNA duplex binding activity by 3-fold. The NMR titration has been performed in duplicate with similar results.

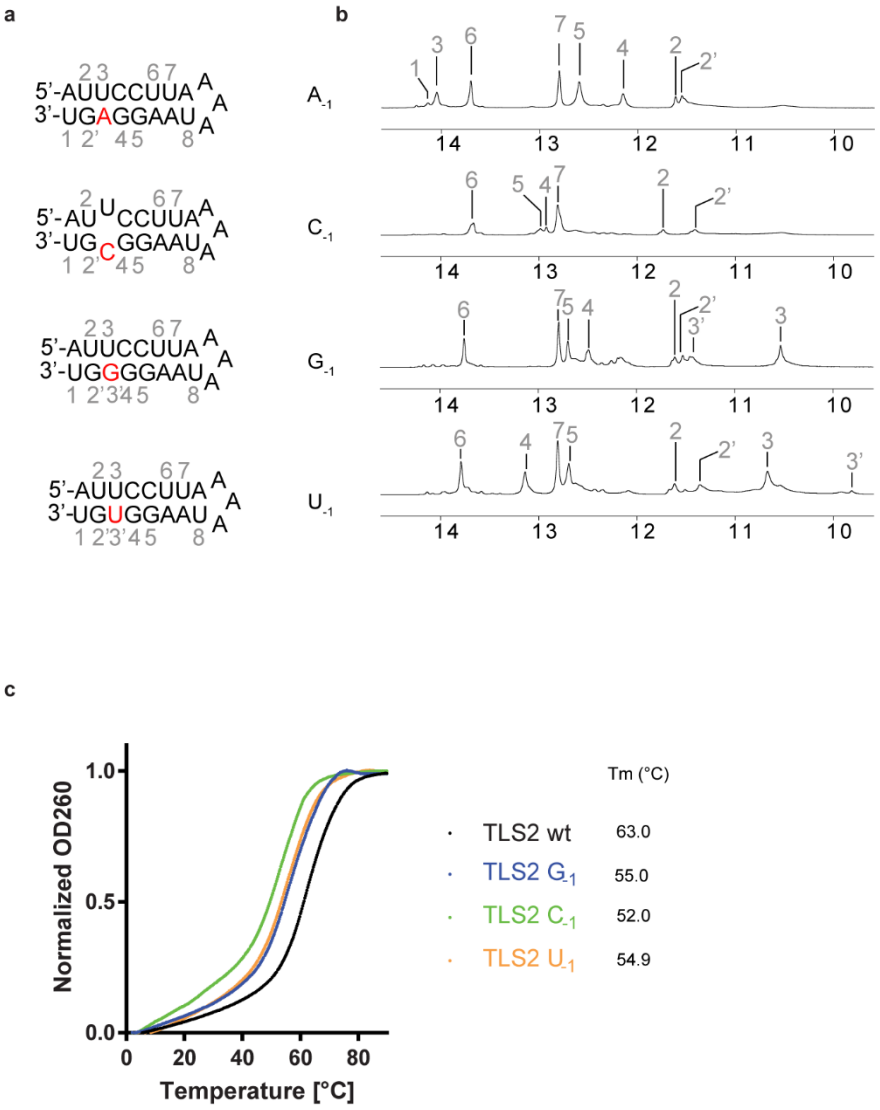


**Supplementary Figure 8 – Analysis of TLS2 variants and effect of SMN-C5 in RNA duplex stabilization. a,** Secondary structures of the TLS2 variants. The position -1 is highlighted in red and the imino protons are numbered in grey. **b,** Portions of 1D $^{1}$H spectra showing the imino region of the four TLS2 variants. This experiment has been recorded a single time. **c,** UV melting curves of the TLS2 variants. These experiments have been recorded in duplicates with similar results.

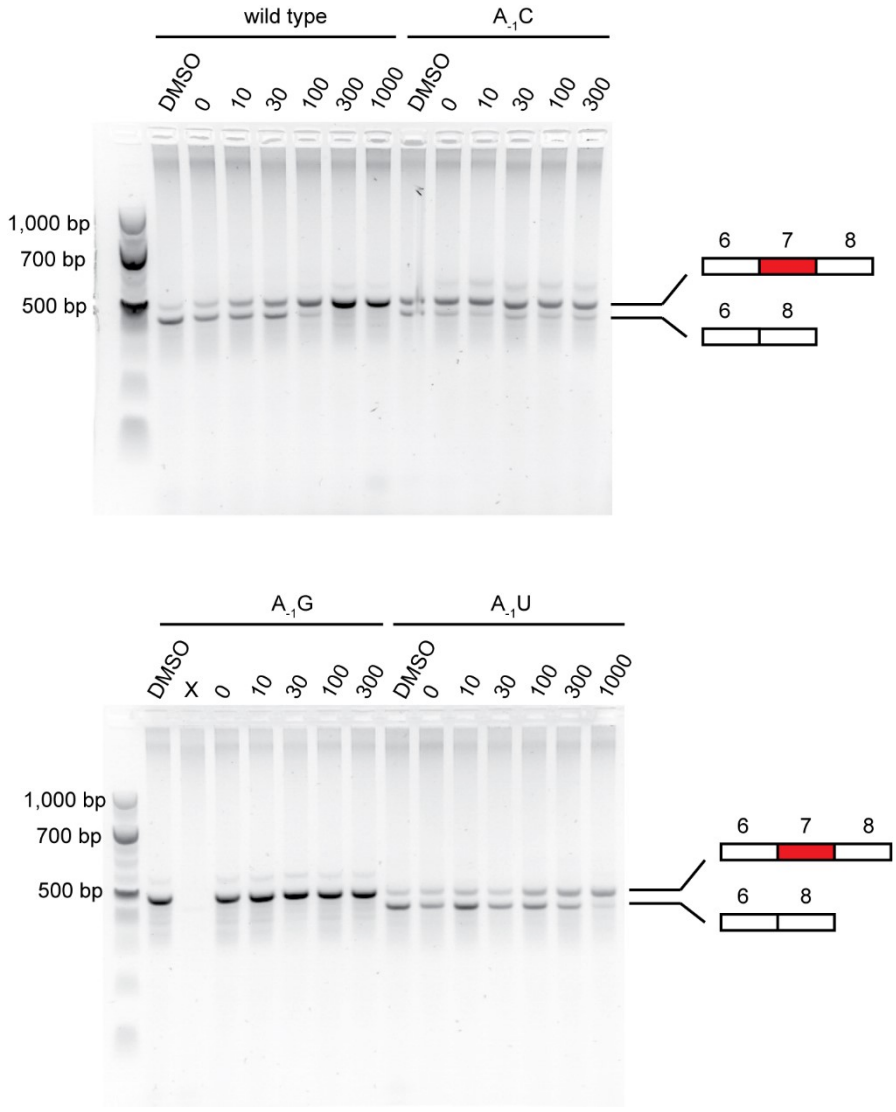


**Supplementary Figure 9 – SMN2 splicing assays shown in figure 3d.** Non cropped gels of the SMN2 splicing assays described in Fig. 3d. On both gels, the first lane corresponds to the size marker. For each construct (wild-type, $A_{-1}C$, $A_{-1}G$ and $A_{-1}U$), the lane labeled DMSO corresponds a control that allow to check for any effect due to DMSO only. Then above each lane, the concentration of SMN-C5 in nM used to incubate the cell is written. For the construct $A_{-1}G$, the lane labeled with a X corresponds to a pipetting error performed when loading the gel.

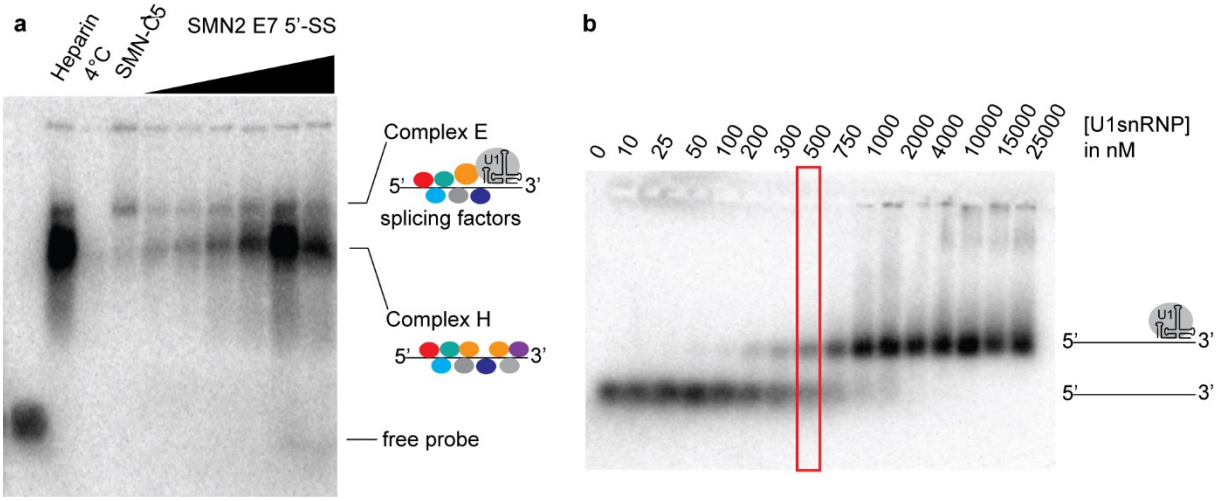


**Supplementary Figure 10 – Electrophoretic mobility shift assays. a**, Autoradiography of the 1% agarose gel showing the two protein-RNA complexes observed when the *SMN2* RNA fragment was incubated with Hela nuclear extract. The most retarded complex corresponds to the E complex since it disappears when the mixture was incubated at 4°C or when either Heparin or cold 5'-SS of E7 were added to the mixture. The E complex is stabilized in presence of SMN-C5. This experiment has been performed two times with similar results. **b**, Autoradiography of the 1% agarose gel showing the binding of *in vitro* reconstituted U1 snRNP on the SMN2 E7 pre-mRNA fragment. The red-squared conditions were chosen to test the effect of SMN-C5 on the binding of U1 snRNP on the pre-mRNA fragment. This experiment has been performed two times with similar results.

**Supplementary movies legends**

**Supplementary movie 1. Solution structure of the apo-RNA duplex.** Ribbon representation of the lowest energy model of the NMR solution structure of the apo-RNA duplex. The U1 snRNA and the E7 5'-SS are colored in gray and blue respectively. The color code for the bases located at the exon-intron junction is the same than in Fig. 2c. The structure is rotating along the RNA helix axis.

**Supplementary movie 2. Solution structure of the RNA duplex bound to SMN-C5.** Ribbon representation of the lowest energy model of the NMR solution structure of the RNA duplex bound to SMN-C5. The U1 snRNA and the E7 5'-SS are colored in gray and blue respectively. The color code for the bases located at the exon-intron junction is the same than in Fig. 2c. The structure is rotating along the RNA helix axis.

**Supplementary movie 3. RNA conformational switch induced by SMN-C5 – Major groove view.** Ribbon representation of the SMN-C5 binding interface of the RNA duplex. The view is centered on the major groove interface of the exon-intron junction. The movie is a morph between the apo-conformation of the RNA duplex on which SMN-C5 was randomly placed outside of the binding interface and the conformation of the complex RNA duplex : SMN-C5. SMN-C5 is displayed as sticks model and colored in yellow. The insertion of SMN-C5 in the major groove triggers the stabilization of $A_{-1}$ in the RNA base stack and the reorganization of the base pairs $G_{+1}$-$C_8$ and $G_{-2}$-$C_9$. This conformational change is further supported by NMR data (Supplementary Figure 1) that shows the broadening of the imino signal of $G_{-2}$ upon SMN-C5 binding.

**Supplementary movie 4. RNA conformational switch induced by SMN-C5 – Minor groove view.** Ribbon representation of the SMN-C5 binding interface of the RNA duplex. The view is centered on the minor groove interface of the exon-intron junction. The movie is a morph between the apo-conformation of the RNA duplex on which SMN-C5 was randomly placed outside of the binding interface and the conformation of the complex RNA duplex : SMN-C5. SMN-C5 is displayed as sticks model and colored in yellow. The insertion of SMN-C5 in the major groove triggers the stabilization of $A_{-1}$ in the RNA base stack and the reorganization of the minor groove that became more accessible for U1-C zinc finger binding.